Zhang, D.-S., *et al.*: Numerical Investigation of Time-Dependent Cloud ...
THERMAL SCIENCE: Year 2016, Vol. 20, No. 3, pp. 913-920

913

NUMERICAL INVESTIGATION OF TIME-DEPENDENT CLOUD CAVITATING FLOW AROUND A HYDROFOIL

by

De-Sheng ZHANG [*], *Guan-Gjian ZHANG, Hai-Yu WANG, and Wei-Dong SHI*

Research Center of Fluid Machinery Engineering and Technology, Jiangsu University,
Zhenjiang, China

Time-dependent cloud cavitation around the 2-D Clark-Y hydrofoil was investigated in this paper based on an improved filter based model and a density correction method. The filter-scale in filter based model simulation was discussed and validated according to the grid size. Numerical results show that in the transition from sheet cavitation to cloud cavitation, the sheet cavity grows slowly to the maximum length during the re-entrant jet develops. The mild shedding bubble cluster convects downwards the hydrofoil and continues to grow up after detaching from the suction surface of hydrofoil, and a bubble cluster introduced at the rear part of hydrofoil. While the sheet cavity generates, the bubble cluster breakups.

Key words: *sheet cavitation, cloud cavitation, hydrofoil, filter based model, density correction method*

Introduction

Cavitation is more like a *protective mechanism* of liquid, preventing local pressure from dropping below the vaporization pressure of the liquid. Early researches on cavitation mainly focused on operational and design issues in the maritime and hydraulic engineering fields [1, 2]. In recent decades, a broader range of topics have been brought in. Cavitation in hydraulic machines often results in erosion damage, transient loads, vibration, noise, and performance decrease by highly unstable behavior of gas-liquid two-phases flow [2-4].

Cavitation model most commonly used nowadays is based on the consumption that the mixture of liquid and vapor phase can be considered as one, which means that two phases share the same velocity and no slip velocity exists between the two phases. Coutier-Delgosha *et al.* [5, 6] assume that barotropic state law governs mixture density, but this may neglect vorticity generation which is crucial for the highly unstable cavitation flow [7, 8]. Another category of cavitation models is based on the first order simplified Rayleigh-Plesset equations, from which interphase mass transfer term between gas and liquid [9-12] is deduced. Morgut and Nobile [13] calibrated the empirical coefficients in Kunz, Zwart, and Singhal cavitation model [9-11], using an optimization strategy for a balance of accuracy and stability.

The objective of this paper is to construct an improved filter based model (FBM) turbulence model on the basis of random number generator (RNG) k-ε turbulence model, coupled

---

with density correction method, and employ it in the study of time-dependent cavitating from sheet cavitation to cloud cavitation around the 2-D Clark-Y hydrofoil.

Improved FBM turbulence model

Inspired by the original idea of FBM model, FBM model based on RNG k-ε has similar expressions:

$$\mu_t = C_\mu \frac{\rho k^2}{\varepsilon} F, \quad F = \min\left(1.0, C_3 \frac{\Delta}{l_{RANS}}\right) \tag{1}$$

where $C_3 = 1.0$. In small turbulence scale region, turbulence viscosity $\mu_t = C_\mu \rho k^2/\varepsilon$, and RNG k-ε turbulence model is used. In area with large turbulence scale, turbulence viscosity $\mu_t = C_\mu \rho \Delta k^{1/2}$, which is actually one-equation large eddy simulation (LES) proposed by Schumann and studied by Yoshizawa [2].

The hybrid method for the filter function, F, and density corrected model (DCM) [5] was added in the kinematic eddy viscosity equation to reduce the turbulent eddy viscosity and limit the over prediction in the cavitating flow over wall of the hydrofoil and in the wake:

$$\mu_{t\ MFBM} = C_\mu \frac{\rho k^2}{\varepsilon} F, \quad F = \min\left(f(n), C_3 \frac{\Delta}{l_{RANS}}\right) \tag{2}$$

$$f(n) = \frac{\rho_v + \alpha_l^n (\rho_l - \rho_v)}{\rho_v + \alpha_l (\rho_l - \rho_v)}, \quad n = 10 \tag{3}$$

It was validated that the FBM model can limit the turbulent eddy viscosity in the cavitating wake of the hydrofoil [5], where the DCM is not effective in reducing the turbulent eddy viscosity because of the high vapor fraction in the shedding cloud cavity.
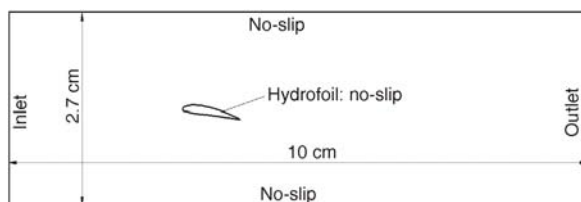

Figure 1. Computational domain

Computational domain, meshing, and boundary conditions

Clark-Y hydrofoil is investigated in this paper, and the experiment of this hydrofoil with chord length $c = 70$ mm, angle of attack $\alpha = 8°$, was conducted by Wang *et al.* [14]. The rectangle computational domain is illustrated in fig. 1, which is installed the same as the experiment set-up. The leading edge is set at the original point of co-ordinates. The distant between upper wall and bottom wall is 2.7 cm, outlet is 10 cm away from inlet and leading edge of hydrofoil is 3 cm from inlet.

The main boundary conditions are set: inlet velocity $U_{in} = 10$ m/s, corresponding Re = $\rho_L c U_{in}/\mu_L = 7 \cdot 10^5$, low inlet turbulence intensity (1%), pressure outlet. No-slip wall is adopted in the upper and bottom wall. The outlet pressure is determined by the cavitation number. During the unsteady calculation, convergence in each physical time step was achieved from 4 to 10 iterations when the root mean square residual dropped below 10^{-5}. The unsteady simulations used time step $\Delta t = 0.1$ ms for the revolution calculation. The medium is water and water vapor in 25 °C, corresponding physical characteristics of water are set: water density $\rho_L = 998$ kg/m³, water dynamic viscosity $\mu_L = 1.139 \cdot 10^{-3}$ Pa·s, saturation pressure of water vapor $p_{sat} = 3574$ Pa, vapor density $\rho_v = 0.02308$ kg/m³, dynamic viscosity of vapor $\mu_v = 9.8626 \cdot 10^{-6}$ Pa·s.

As shown in fig. 2, structured grid is established in the computation domain. A C-type block was used around the hydrofoil, considering the round shape in head of hydrofoil and the sharp rear part. Three grids are generated to evaluate the grid independence as shown in tab. 1.
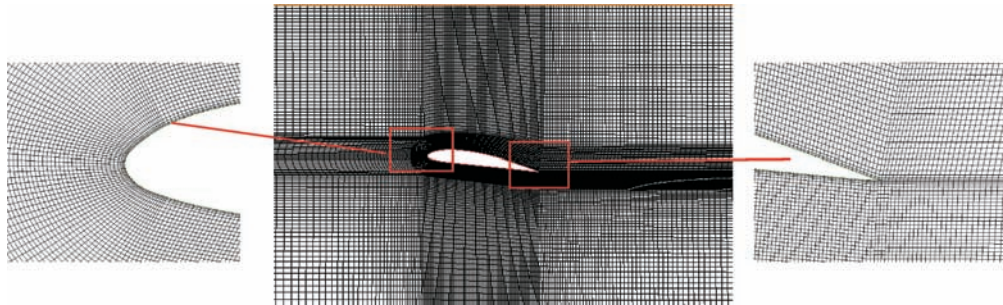

Figure 2. Overall mesh around Clark-Y hydrofoil

Table 1. Predicted calculated by different grids

Grid	Nods number	C_{pmax}	C_L	C_D
Coarse 1	30502	1.02	1.200	0.041
Medium 2	59673	1.11	1.150	0.038
Refined 3	118321	1.13	1.140	0.038
Experiment [5]	–	1.20	1.152	0.037

As shown in tab.1, the medium density grid has nearly the same result with fine grid, and consists with experimental results as well. Considering the large velocity gradient at the head of hydrofoil and the complex flow in the wake of hydrofoil, mesh is intensified in areas previously mentioned as show in fig. 2. The value of y^+ for medium grid varies between 40~100, with an average of 71.

Determination of filter scale in FBM

The FBM combines the advantages of RANS and LES equations, but it requires a reasonable filter scale, Δ. When filter scale Δ is very small, FBM is almost one-equation LES model, resulting in enlarge grid number and computational resources. In order to acquire a proper filter scale Δ, we tested $0.7\,L$, $1.01\,L$, $2.0\,L$, $4.0\,L$, and RANS (infinity L) in unsteady cavitation simulation around Clark-Y with a cavitation number $\sigma = 0.8$. The monitoring location is at the $1.2c$ down-stream of hydrofoil leading edge, shown as the fig. 3. The numerical results show that smaller the filter scale becomes the more massive bubble cloud shedding is obtained and the interface of liquid and vapor tends to be fractured. However, the resolution will not improve continuously without a refined grid. Time averaged lift and drag coefficients in five cycles are presented in tab. 2, in which both coefficients are approaching the experimental results. The time-average velocity profile of different numerical simulation model are compared with the experiment data when the FBM filter scale is reduced to $0.70\,L$, the prediction data tend to be stable as shown in fig. 4.

Consequently, a proper filter scale is critical to the precision of calculation. A smaller filter scale increases FBM capacity to resolve smaller scale vortex. However, it is not linear and also limited by the grid scale. Thus, filter scale $\Delta = 1.01\,L$ was finally used in the present study.
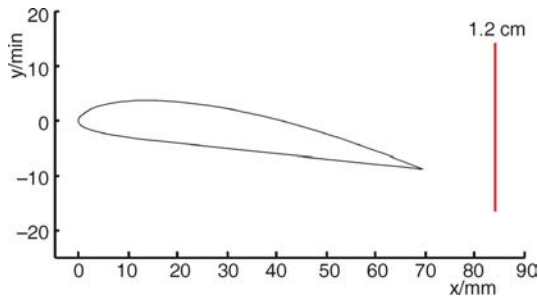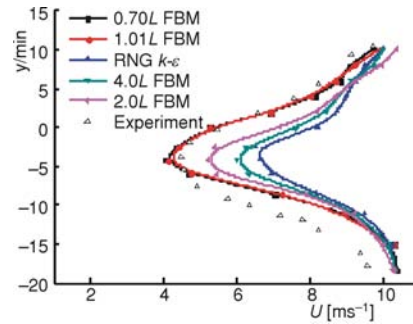
Figure 3. Monitoring location

Figure 4. Time-averaged velocity U at $x = 1.2$ cm

Table 2. The average lift and drag coefficients computed with different filter sizes

	RNG k-ε	4.0L	2.0L	1.01L	0.70L	Experiment [5]
C_L	0.693	0.702	0.719	0.735	0.738	0.760
C_D	0.109	0.112	0.113	0.115	0.115	0.119

Results and discussion

As shown in fig. 5, when cavitation number, σ, decreases to 1.2, sheet cavity starts to be unsteady. Particularly, massive bubble cluster sheds from the rear part of closure, indicating that cavitation is converting from quasi-steady sheet cavitation to quasi-periodic cloud cavitation. The time averaged lift and drag coefficients of transition stage are 0.982 and 0.064, respectively. The period is approximately 65.3 ms. The cavity evolution in one typical period is presented in fig. 5. The time averaged lift coefficient is 0.982 and drag coefficient is 0.064, with a period time $T = 65.3$ ms. Cavity grow slowly in figs. 5(a)-(c) to the maximum length 0.4 cm and the re-entrant jet develops at the same time. In fig. 5(d), when re-entrant jet is strong enough to force the cavity back to the head of hydrofoil, primary shedding occurs. In figs. 5(e)-(g), the primary shedding, A, moves downwards the hydrofoil with a velocity of 2.23 m/s, which is smaller than the main flow velocity 10 m/s. Bubble cluster, A, continues to grow up after shedding off and induces a bubble cluster, B, in fig. 5(h), when A passes the trailing edge of hydrofoil. Sheet cavity grows up again in fig. 5(i) and shrinks in the following three figures, during which bubble B expands at first and breakup. The pressure wave degenerates the sheet cavity at the leading edge of hydrofoil temporarily. Sheet cavity oscillates and develops again in another cycle in fig. 5(m)-(p).

Lift coefficients, vapor volume and pressure coefficients are given in fig. 6. One typical period is divided into four phases by five dashed lines. Phase 1 corresponds to (a)-(e) in fig. 5, in which growth and oscillation of cavity dominate most of time, and primary shedding occurs at the end of phase. In this phase, lift coefficient inclines steadily. The pressure on suction side, at chord ratio $x/c = 0.1$, keeps low 3574 Pa, which is the saturation pressure of vapor. As the maximum length of cavity is about 0.4 cm and continues to grow, pressure at $x/c = 0.5$ persist declining.

However, pressure at $x/c = 0.9$ remains high without much fluctuation since it's far from cavity. Phase 2 corresponds to (f)-(h) in fig. 5, in which vapor volume ascends dramatically attributing to the expansion of detached bubble A and development of bubble B induced by vortex at rear part of hydrofoil. At the same time, lift coefficient drops rapidly because of the bubble shedding. Influenced by the rear part bubble, pressure at $x/c = 0.9$ decreases severely. From phases 1
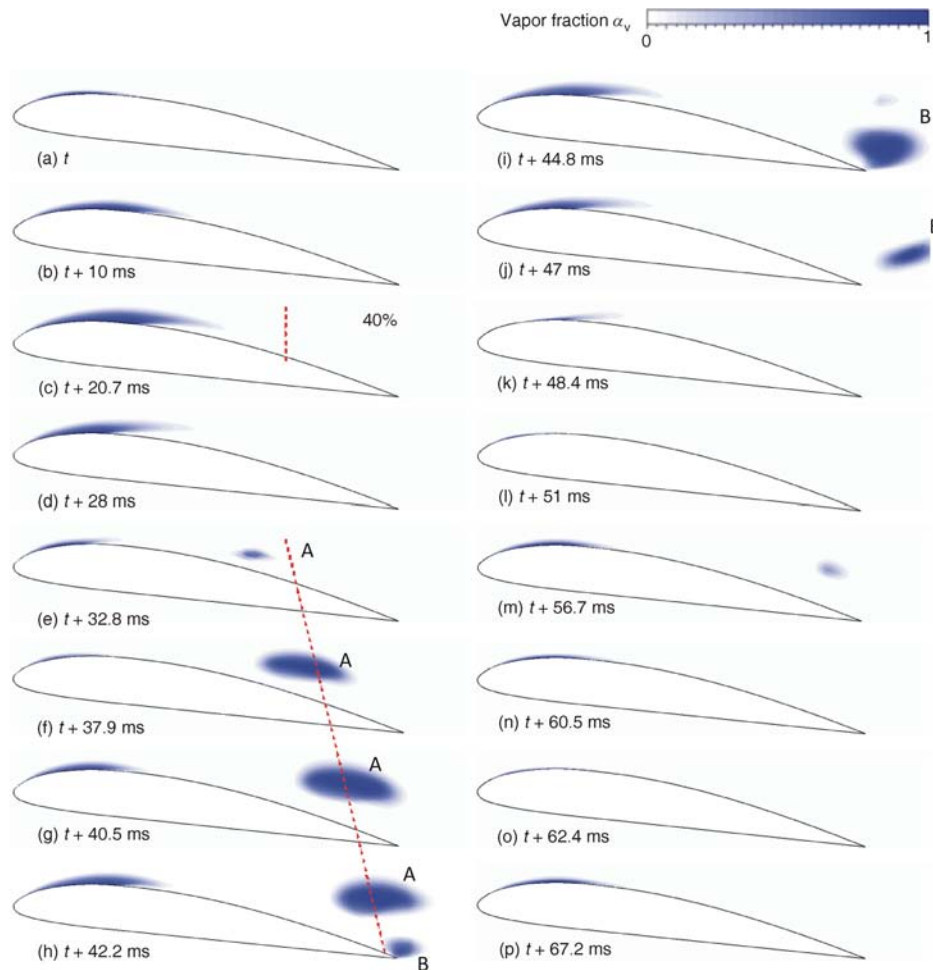
Figure 5. Simulation results of cavity evolution in transition stage in one typical period, $\sigma = 1.2$

and 2, it's observed that there is a lag between the variable vapor volume and the pressure fluctuation as well as the lift coefficient. The former is always slightly slower than the latter for the cavity is pressure field driven and the bubble needs time to generate or degenerate. Phase 3 corresponds to (i)-(k) in fig. 5, in which primary shedding bubble A and rear part bubble B collapse when they move toward the high pressure region. Consequently, vapor volume decreases dramatically and lift coefficient tends to go up. When the primary bubble collapses, an extremely high pressure wave occurs in the pressure field, which is presented by high peaks in pressure at $x/c = 0.1$, 0.5, 0.9. Lift coefficient promptly jumps to the lowest because of this pressure wave. Phase 4 corresponds to (l)-(p) in fig. 5, in which it's free of cavity on the suction side of hydrofoil at first, impacted by the pressure wave, and cavity grows and oscillates again later.

Three vertical lines is arranged at $x = 0.4$, 0.8, and 1.2 cm to detect the time averaged horizontal velocity, u, in condition of non-cavitation, $\sigma = 1.4$ and $\sigma = 1.2$ illustrated in fig. 7(a).

In the non-cavitation simulation result, the viscous layer near wall shows large velocity gradient influenced by wall at $x/c = 0.4$ and 0.8. However, time-averaged velocity, u, ap-
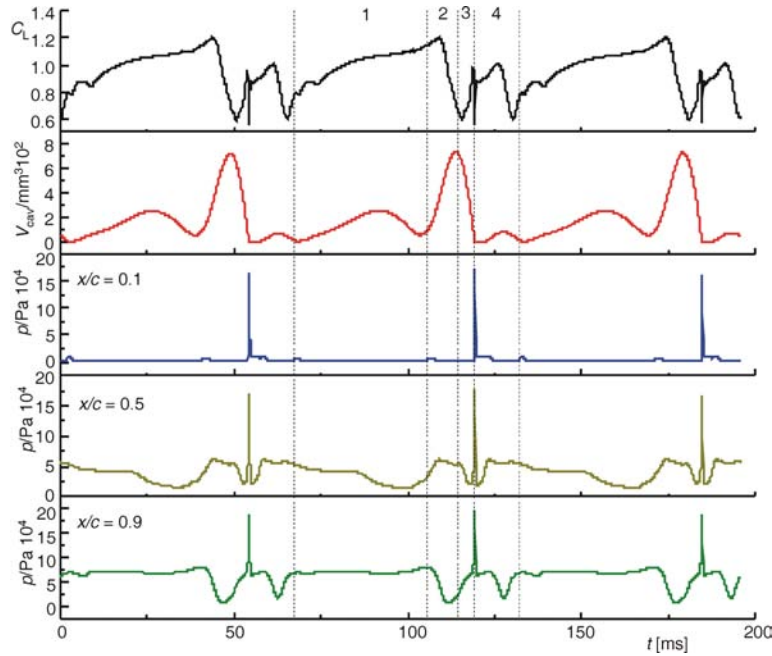
Zhang, D.-S., *et al.*: Zhant, D.-S., *et al.*: Numerical Investigation of Time-Dependent Cloud ...

918　　　　THERMAL SCIENCE: Year 2016, Vol. 20, No. 3, pp. 913-920

Figure 6. Time evolution of lift coefficient, total cavity volume and pressure coefficients in three cycles
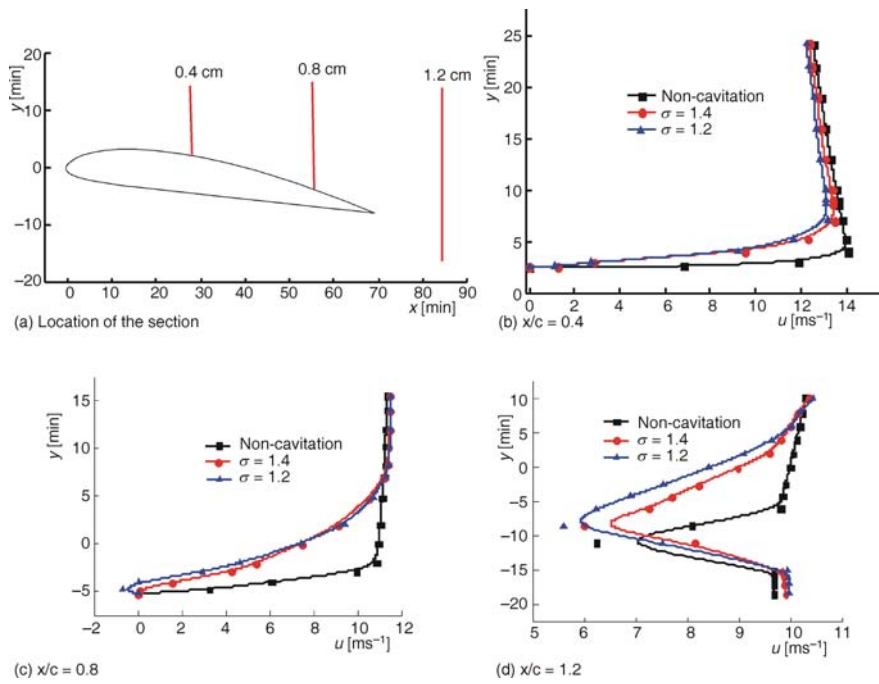

Figure 7. Comparison of time averaged horizontal velocity at different locations with various cavitation numbers

proaches main flow velocity 10 m/s outside the viscous layer. The boundary layer at $x/c = 0.8$ is thicker than that at $x/c = 0.4$ but still remains attached. As shown in the fig. 7(a) $x/c = 1.2$ locates in the wake of hydrofoil, a profound low velocity occurs. When cavitation is activated, the boundary layer near hydrofoil surface is significantly impacted. The boundary layer at $x/c = 0.4$ and 0.8 becomes thicker in a large degree, and tends to separate. When cavitation number $\sigma = 1.2$, averaged horizontal velocity at $x/c = 0.8$ decreases to negative, which is a solid evidence of adverse re-entrant jet. Intensity and area of re-entrant jet tends to be enhanced and expanded with the decrease of cavitation number. The strong unsteady characteristics including the primary shedding have presented in the transition from sheet cavitation to cloud cavitation.

Conclusions

An improved FBM model combining RNG k-ε and one equation LES, together with additional density correction is proposed and validated in this paper. The filter scale, Δ, is tested and selected properly on the basis of grid scale to validate the prediction accuracy.
The sheet cavity grows slowly to the maximum length 0.4 cm at cavitation number $\sigma = 1.2$, during re-entrant jet develops at the same time. When re-entrant jet is strong enough to force the cavity back to the head of hydrofoil, primary shedding occurs. The primary shedding bubble A flows downwards the hydrofoil and continues to grow up after shedding off and induces a bubble cluster B at rear part of hydrofoil. While sheet cavity oscillates and generates, bubble cluster B breakups.
The velocity profile of non-cavitation, cavitation $\sigma = 1.2$ and 1.4 were simulated to explain the reason of the re-entrance jet flow which induces the shedding cavitation.

Acknowledgment

References

[1] Arndt, R. E., Cavitation Research from an International Perspective, *Proceedings*, IOP Conference Series: Earth and Environmental Science, IOP Publishing, Beijing, 2012, Vol. 15, Part 1, 012002
[2] Arndt, R. E., Some Remarks on Hydrofoil Cavitation, *Journal of Hydrodynamics, Ser. B, 24* (2012), 3, pp. 305-314
[3] Brennen, C. E., *Cavitation and Bubble Dynamics*, Cambridge University Press, Cambridge, UK, 2013
[4] Brennen, C. E., *Hydrodynamics of Pumps*, Cambridge University Press, Cambridge, UK, 2011
[5] Coutier-Delgosha, O., *et al*., Legoupil, Analysis of Cavitating Flow Structure by Experimental and Numerical Investigations, *Journal of Fluid Mechanics, 578* (2007), May, pp. 171-222
[6] Coutier-Delgosha, O., *et al*., Numerical Simulation of the Unsteady Behaviour of Cavitating Flows, *International Journal for Numerical Methods in Fluids, 42* (2003), 5, pp. 527-548
[7] Senocak, I., Shyy, W., Evaluations of Cavitation Models for Navier-Stokes Computations, *Proceedings*, ASME 2002 Joint US-European Fluids Engineering Division Conference, American Society of Mechanical Engineers, Montreal, Que., Canada, 2002, Vol. 1, pp. 395-401
[8] Gopalan, S., Katz, J., Flow Structure and Modeling Issues in the Closure Region of Attached Cavitation, *Physics of Fluids, 12* (2000), 4, pp. 895-911
[9] Kunz, R. F., *et al*., A Preconditioned Navier-Stokes Method for Two-Phase Flows with Application to Cavitation Prediction, *Computers & Fluids, 29* (2000), 8, pp. 849-875
[10] Singhal, A. K., *et al*., Mathematical Basis and Validation of the Full Cavitation Model, *Journal of Fluids Engineering, 124* (2002), 3, pp. 617-624

[11] Zwart, P. J., *et al.*, A Two-Phase Flow Model for Predicting Cavitation Dynamics, *Proceedings*, 5th International Conference on Multiphase Flow, Yokohama, Japan, 2004
[12] Schnerr, G., Sauer, J., Physical and Numerical Modeling of Unsteady Cavitation Dynamics, *Proceedings*, 4th International Conference on Multiphase Flow, New Orleans, La., USA, 2001
[13] Morgut, M., Nobile, E., Numerical Predictions of Cavitating Flow around Model Scale Propellers by CFD and Advanced Model Calibration, *International Journal of Rotating Machinery, 2012* (2012), ID618180, p. 11
[14] Wang, G., *et al.*, Dynamics of Attached Turbulent Cavitating Flows, *Progress in Aerospace Sciences, 37* (2001), 6, pp. 551-581